Yu.V. MILMAN [1,*]**, B.M. MORDYUK** [2, **]**,
K.E. GRINKEVYCH [1]**, S.I. CHUGUNOVA** [1]**,
I.V. GONCHAROVA [1]**, A.I. LUKYANOV** [1]**, and D.A. LESYK** [3]

[1] I.M. Frantsevich Institute for Problems in Materials Science of the N.A.S.
   of Ukraine, 3 Academician Krzhizhanovsky Str., UA-03142 Kyiv, Ukraine
[2] G.V. Kurdyumov Institute for Metal Physics of the N.A.S. of Ukraine,
   36 Academician Vernadsky Blvd., UA-03142 Kyiv, Ukraine
[3] National Technical University of Ukraine 'Igor Sikorsky Kyiv Polytechnic
   Institute', 37 Peremohy Ave., UA-03056 Kyiv, Ukraine

* milman@ipms.kiev.ua, ** mordyuk@imp.kiev.ua

NEW OPPORTUNITIES TO DETERMINE THE RATE OF WEAR OF MATERIALS AT FRICTION BY THE INDENTATION DATA

The article is concerned with the determination of physical plasticity δ_H (the ratio of the plastic strain to the total strain) and yield stress σ_S by indentation and the application of these characteristics for analysis of the wear rate W during the friction. The experimental part of the work is performed on the AISI O2 and AISI D2 steels, the surface layers of which were hardened by combined thermomechanical treatment consisted of sequential use of laser heat treatment and ultrasonic impact treatment. For the metals, W is shown to be proportional to δ_H and inversely proportional to σ_S. The general scheme for the dependence of W on δ_H is proposed and based on experimental results for tool steels and hard alloys. For the steels, whose wear is caused by the plastic deformation, W increases with increasing δ_H, and it decreases conversely for hard alloys worn predominantly by the fracture mechanism. The use of physical plasticity δ_H and yield stress σ_S, which are calculated using the hardness and Young's modulus, characterizes both the hardening extent and the wear rate of the surface layers in more full measure and more accurately than the hardness magnitude itself.

Keywords: wear, physical plasticity, yield stress, hardened surface layer, hardness, indentation.

1. Introduction

The scientific and technical interest in the creation of wear-resistant surfaces is brought about by the fact that the wear during friction is one of the most important mechanical properties that determine the working capacity of a material [1–3]. Currently, steels remain the indispensable materials for numerous applications like railways, bridges, pipelines, and others, where steel products and structures still are the main constituents. Therefore, the prolongation of the operation life of the steel constructions by prevention their degradation under wear/fatigue loading still is a timely and important task.

In practice, the steel may be subjected to a complex combination of conditions where hardness alone may not be sufficient to ensure tribological performance [4–7]. A number of the mechanical and metallurgical parameters, such as the quantity/distribution of Carbon, size/morphology of phases and microstructural elements, work-hardening behaviour, and fracture toughness, were shown can control the wear resistance of steels [1–8]. Therefore, these parameters affecting the wear mechanisms [1–3, 9–11] should be thoroughly considered.

The afore-mentioned parameters were shown can be improved either by the formation of the modified surface layers using various thermal treatments [5, 6, 12–14] and mechanical influences [7, 8, 14–18] or by the production of wear-resistant coatings [19–23].

Several well-known techniques are normally used for evaluation of the wear performance, *viz*., the reciprocating sliding wear test [14, 17, 18, 23], the pin/ball-on-disk method for abrasive wear [12, 21], fretting wear testing [6], *etc*. At the same time, the indentation method allowing determination of mechanical properties of the worn material can also be used for the assessment of the wear resistance [18].

The mechanical behaviour of materials, including wear, should be described using both plasticity and strength characteristics. The wear process of steels and most metallic alloys is determined mainly by their plastic deformation. Therefore, formulas describing the wear rate W should include the plasticity characteristic of the material. However, the elongation to fracture δ widely used in the technique for assessing plasticity (as well as a transversal reduction in the area to fracture) does not correspond to the scientific definition of plasticity in physics and mechanics [24]. The elongation to fracture δ depends not only on the material plasticity but also on many other material parameters: the yield stress σ_S, tensile strength σf, the difference '$\sigma_f - \sigma_S$', strain hardening $d\sigma/d\varepsilon_t$ (where εt is the total strain of the material) and the parameter m, which determines the strain sensitivity of the yield stress.

In addition, the plasticity δ value can only be determined by standard tensile tests. The δ value cannot be determined by indentation,

which is necessary when studying the wear of materials covered by the hardened surface layers or coating. For many high-strength materials, $\delta = 0$ that excludes the possibility of using this characteristic to describe the wear process of these materials. All these reasons led to the lack of plasticity characteristics in the formulas used for calculating the wear of materials.

The authors propose to use for studying the wear rate the physical plasticity δ_H, which is equal to the ratio of plastic strain to total strain. It is easily determined by the indentation method, it corresponds to the scientific definition of plasticity, and it is successfully used in other areas.

Thus, the physical plasticity δ_H was used to elucidate the influence of the electronic structure of covalent crystals on their plasticity [25], to search for the relationship between the plasticity and other physical properties [26], and even to study the effect of plasticity on the wear rate of hard metals [27]. The use of physical plasticity made it possible to introduce the concept of the theoretical plasticity of materials as a development of the concept of theoretical strength [24]. Physical plasticity δ_H was introduced, and the methodology for determining the δ_H was developed in [28–30], and it is used to characterize the plasticity of materials both by the authors of this article and by several other scientists, *e.g.*, in Refs. [24–31]. Physical plasticity δ_H is defined as the ratio of plastic strain to the total strain:

$$\delta_H = \varepsilon_p/\varepsilon_t. \tag{1}$$

In this case, the plastic strain εp, the total strain εt, and the elastic strain εe are determined in the direction of the applied load and the following equation holds $\varepsilon_t = \varepsilon_e + \varepsilon_p$.

To characterize the strength of materials under various types of loads, it is most expedient to use the yield stress of materials σ_S. Since the yield stress of the surface layers, which determine the wear at friction, can significantly differ from the yield stress of the base metal (due to the presence of thin coatings or hardened layers), in most cases, the hardness value H is taken as the strength characteristic when studying the wear of materials. It is most advisable to use Meyer's hardness HM, which has a clear physical meaning of the average contact pressure. The use of HM to characterize strength is usually justified by the Tabor's formula

$$HM = C\sigma_S, \tag{2}$$

where the Tabor's parameter C is taken to be a value independent on the structural state of the materials. On the contrary, it was shown in [29] that C is almost completely determined by the physical plasticity δ_H of material, and, therefore, depends on the structure of the material. Therefore, it is more correct to use the yield stress σ_S rather than the hardness

of the material. To calculate σ_S from the magnitude of the HM, it is necessary to determine the Tabor parameter C. The authors of the article suggest a simple method for calculating the parameter C from the value of δ_H and the subsequent calculation of σ_S according to Eq. (2).

We also note that physical plasticity can be determined both by indentation and by standard mechanical tensile and compression tests. Naturally, to study the wear process during friction, the authors of the article propose to determine the physical plasticity δ_H by the indentation method.

Mechanical properties and wear at friction of the surface layers play a determinative role in the operating characteristics of most metallic products made of steels and other metallic alloys. Therefore, the surface hardening methods, which comprise severe plastic deformation, thermal influence, or the combination of the above, are intensively developing [31–33].

The most effective methods are the sequential or simultaneous application of mechanical surface deformation and thermal influences such as friction stir processing [33], shot peening [34], surface mechanical attrition treatment (SMAT) [8, 35], ultrasonic impact treatment (UIT) (peening) [15–17, 36, 37] or ultrasonic nanocrystal surface modification [38]), and laser-induced hardening due to laser surface melting/alloying [13, 32, 39], laser heat treatment [14], and laser shot peening [17, 40–42]. Occurred microstructural modifications such as grain refinement [8, 15, 34, 35], formation of gradient microstructure [38], phase transformations [15, 38], carbide dissolution/precipitation [39, 14], fixation of grain boundaries [14, 43] may provide essential enhancement in the surface layers properties.

Thus, an improvement of the measurement methodologies and prognosis of mechanical properties of the hardened layers (and thin coatings) including their friction wear is an important practical task. It can be solved only with the use of modern achievements in the physics of indentation into account.

Unfortunately, a vast majority of the scientific works considers and assesses mechanical properties of hardened surface layers and thin coatings based on their hardness only. As known, the mechanical behaviour of a material can only be characterized, if both its yield stress and plasticity would be determined. Therefore, it is advisable to characterize the mechanical properties of the hardened surface layers and wear rate at friction by the magnitudes of the yield stress σ_S and the physical plasticity δ_H. Both σ_S and δ_H can be easily determined by the indentation methods, *viz.* microindentation or nanoindentation.

This article aims to develop an approach for determination of the yield stress σ_S and the physical plasticity δ_H on the base of the Meyer hardness (HM) and their application for the description of the wear rate

at friction. Applicability of the suggested methodology is illustrated by the experimentally obtained wear rate W of the samples of AISI O2 and AISI D2 steels in the initial state and covered by the hardened surface layers. The optimal value of the physical plasticity δ_H for the hardened surface layers was determined. New physical regularities for the friction wear were elaborated and discussed.

2. Mechanical Properties of Materials Determined by the Indentation Method

2.1. Determination of Physical Plasticity

In modern physics and mechanics, plasticity is considered as the ability of a material to be irreversibly (plastically) deformed under the load applied [24]. The widely used plasticity characteristics, such as the elongation before fracture during a tensile test (δ) or the area reduction before fracture (ψ), do not meet this definition. As a result, despite many decades of use of δ and ψ, no theories of their dependence on structural parameters of material, temperature, and strain rate were developed. Such a situation greatly delayed the practical work aimed to increase the materials' plasticity.

The physical plasticity characteristic, δ_H, was proposed in Ref. [28] as the fraction of plastic strain ε_p in total strain ε_t in the direction of the applied load (see Eq. (1)). It is seen from Eq. (1) that the physical plasticity δ_H is a dimensionless quantity, which can take the magnitudes ranged within the interval: $0 \leq \delta_H < 1$.

The δ_H quantity corresponds to the physical definition of plasticity and can be determined by standard mechanical tensile or compression tests, as well as by the hardness measurements.

It was shown in Refs. [29, 30] that for the Vickers pyramidal indenter (the angle between the face and the axis of the pyramidal indenter is $\gamma = 68°$):

$$\delta_H = 1 - 14.3\left(1 - \nu - 2\nu^2\right)\frac{HV}{E}, \tag{3}$$

where HV, E, and ν are respectively Vickers hardness, Young's modulus, and Poisson's ratio of the investigated material.

For metallic alloys, the value of δ_H can be determined in the wide temperature range including cryogenic temperatures. The value of δ_H was determined for materials with different interatomic forces, including covalent crystals [29].

The physical plasticity can also be determined using the nanoindentation method [24, 27, 44–46]. For the physical plasticity δ_H, unlike the plasticity δ, a theory, which describes the effects of structural state (grain size, dislocation density, disperse reinforcing particles) on δ_H,

exists. It allows one to choose the appropriate structural state of a material to obtain an optimal yield stress/plasticity ratio [24, 28].

2.2. The Yield Stress Determination

There are several theories for the indentation process that allow assessing the yield stress value σ_S using the hardness magnitude [44, 47–50].

We think that to determine the yield stress and Tabor parameter C precisely it is expedient to use the inclusion core model, describing the indentation process, developed by Johnson [49] and improved in [29]. A system of three equations was obtained in Ref. [29]. Solving the system, we can rather accurately determine the magnitudes of C and σ_S. A simplified methodology of the σ_S determination, which can be used for practical purposes, was also suggested [29].

Analysis of a great number of materials with different crystalline structures and different types of interatomic interaction allowed revealing the correlation dependence between the Tabor parameter C and the plasticity characteristic δ_H (Fig. 1). Moreover, the $\delta_H(C)$ dependence was revealed to be theoretically described.

The theoretical dependence of $\delta_H(C)$ for pyramidal indenters obtained in Ref. [29] contains parameter C in the implicit form:

$$\delta_H = 1 - \frac{2.21\, z\, C\, \lambda}{\exp(1.5\, C - 1) - \alpha}, \quad (4)$$

where

$$\alpha = 1 - \frac{2(1 - 2\nu)}{3(1 - \nu)},$$

$$\lambda = \frac{1 - \nu - 2\nu^2}{1 - \nu},$$

$$z = \cot\gamma - \frac{2HM(1 - \nu_i)}{E_i},$$

and E_i is the Young modulus of the indenter.

Fig. 1. Relationship between the Tabor parameter $C = HM/\sigma_S$ and the physical plasticity δ_H. Results obtained for steels (the initial (*1*, *2*) and hardened (*3*, *4*) samples of AISI O2 (*1*, *4*) and AISI D2 (*2*, *3*) steels) in this study are added to the graph plotted in Ref. [29]
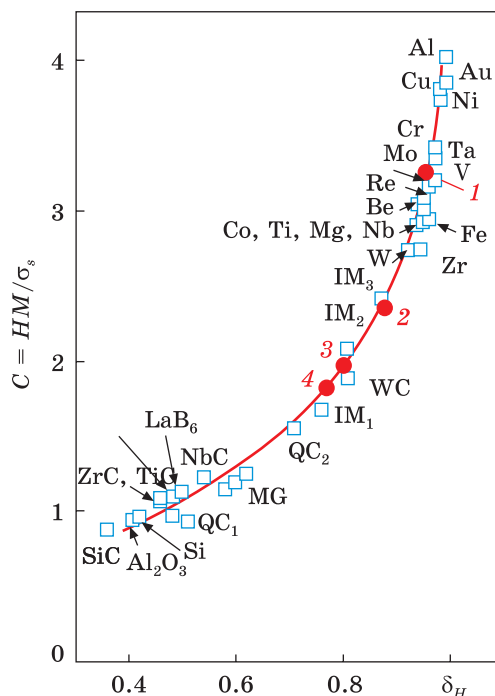
Table 1. **The chemical composition of the studied steels (in wt.%)**

Material	C	Mn	Si	V	Cr	Mo	Ni	Cu	Fe
AISI O2	0.9	2.0	0.3	0.2	–	–	0.4	0.3	Bal.
AISI D2	1.15	0.46	0.6	0.72	11.3	0.83	0.15	0.06	Bal.

Parameter C can be easily evaluated using Eq. (4) employing and standard computer-aided math-programs.

The simplified methodology for the yield stress evaluation involves a preliminary determination of the plasticity characteristic δ_H by using the simple formula (3), and the Tabor parameter C using the formula (4). Moreover, parameter C could be estimated from the graph $C(\delta_H)$ (Fig. 1), then the yield stress would be easily calculated using Eq. (1), *i.e.* $\sigma_S = HM/C$. The latter methodology of the σ_S determination takes very little time, and it was validated to give the results of sufficient practical accuracy.

3. Materials and Experimental Details

3.1. Material

The chemical compositions of the AISI O2 and AISI D2 steels used for experimental studies are given in Table 1. The mechanical properties of the surface layers on the samples of these two steels in initial states and after surface hardening were determined by the indentation method.

3.2. Surface Modification Technique

An effective method for hardening the surface layers of steels, which was developed and tested in [14, 51, 52], was used in this work. This method comprises a combination of laser heat treatment (LHT) and ultrasonic impact treatment (UIT) to perform the combined hardening process. The strongly hardened surface layers on the AISI O2 and AISI D2 steels can be obtained using the appropriate regimes of LHT and UIT processes reported in [14].

It is of importance that the complexly hardened (LHT + UIT) surface layers of the AISI O2 and AISI D2 steels samples contain the stable dislocation/subgrain structures. It allowed avoiding structural changes during the wear tests when these samples were used to collect the data of the tribological tests and to study the influence of the physical plasticity δ_H and yield stress σ_S on the wear rate of materials during friction.

3.3. Microstructure Examination Methods

The x-ray diffraction (XRD) analysis of the surface layers of about 10–20 μm thick was carried out using a DRON-3M diffractometer in CuK_α radiation. The changes in the peak broadening β were analysed to evalu-

ate the lattice microstrains and the size of the coherent scattering areas (CSA). A JEOL-CX-II 100 transmission electron microscope (TEM) was used to observe the microstructures of the samples. The plane-view TEM foils from the top surface layer ≈5–8 μm below the outmost surface obtained by one-side polishing were analysed.

3.4. Hardness and Wear Rate Assessment Techniques

The microhardness of the steel samples in the initial and hardened states was determined using a PMT-3 instrument equipped with a Vickers indenter at a load of 0.5 N. To study the hardness depth profile in the samples with the hardened surface layers, the sample sections were made at an angle of 35° to the surface planes, and microhardness was measured at a load of 0.2 N in this case.

Tribological properties of the plane samples were evaluated using an automated tribological complex [14] on the base of the analysis of the reciprocating sliding of spherical indenter made of hard alloy (94% of WC, 6% of Co) in the industrial oil (*I*-20) environment. The sliding velocity and distance were 0.013 m/s and 11.7 m, respectively. The indenter diameter was 8 mm, its hardness was ≈94 *HRA*. The wear data for each material were obtained on the base of the three statistically averaged runs. The reproducibility of tribomeasurements of the tests under the specified contacting scheme was ≈4%.

The wear rate W of the material during the friction process was characterized by the depth of the friction groove. The profiles of the wear tracks were registered using P-201 profilograph–profilometer with a systematic (instrumental) error of 0.1 μm. The friction plasticity coefficient K_f was also determined as the ratio of the cross-sectional area S_2 of two pile-ups formed along the friction groove to the cross-sectional area of the friction groove S_1 [53, 54]:

$$K_f = S_2/S_1. \tag{5}$$

As supposed in Ref. [55], $0 < K_f < 1$, and parameter K_f can take values 1 or 0 in the boundary cases when either ideal material removal without pile-ups' forming ($K_f = 0$) or conversely the ideal ploughing accompanied with no material removal $K_f = 1$) is observed. On the practice, the magnitude of K_f is always lower than 1.

4. Results and Discussions

4.1. Microstructure Observations

According to XRD and TEM analysis, the microstructure of the initial AISI O2 and AISI D2 steel samples contains relatively large (0.5–2 μm) ferritic-pearlitic and austenitic (≈10%) grains, and primary VC carbides
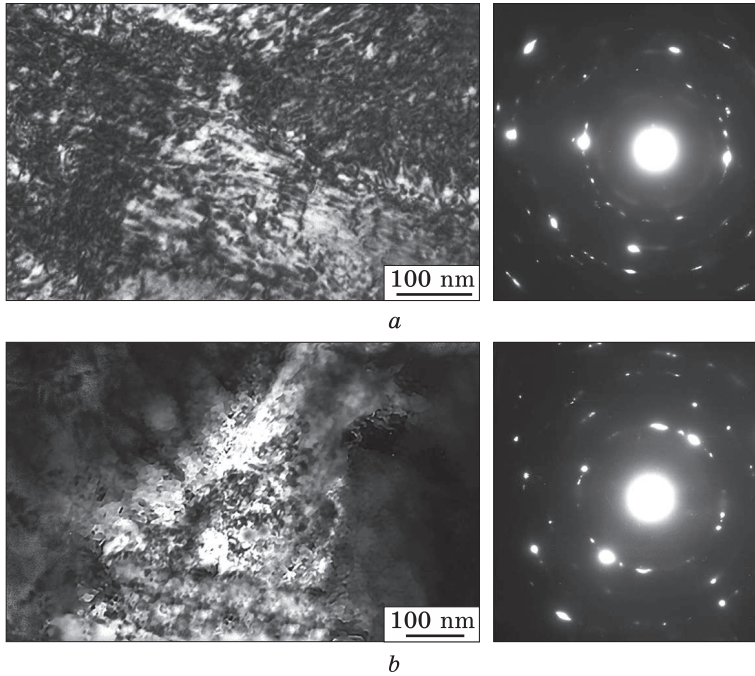
Fig. 2. Typical TEM bright-field images of microstructures and SAED patterns of the combined LHT + UIT processed layers of the AISI O2 (*a*) AISI D2 (*b*) tool steels

(AISI O2) and VC, Cr_7C_3 and $Cr_{23}C_6$ carbides (AISI D2). The initial AISI D2 steel possesses some non-homogeneity of chromium carbides (undesirable coagulation might result in the carbide coarsening to ≈5−10 μm) [14]. The combined LHT + UIT processing applied led to essential microstructural changes and phase rearrangements in the surface layers of both studied steels. The examples of the dislocation/subgrain structures observed in the strongly hardened surface layers investigated in this paper are shown in Fig. 2. Microstructures of the hardened layers of both steel samples contain a mixture of fragmented ferrite with small grains and subgrains and fine secondary carbides. XRD analysis respectively gives the grain size (CSA size) of 40−80 nm and ≈120−150 nm for AISI O2 and AISI D2 steels. The character of the selective area electron diffraction (SAED) patterns indicates the presence of high-angle misorientations between the structural elements. Sometimes, the bundles of deformed ferritic/pearlitic/martensitic plates can be found (Fig. 2, *a*).

It is of special importance that these microstructures are stable to external influences owing to the existence of uniformly dispersed fine (of 20−60 nm) carbides that fixed both the dislocations and grain/subgrain boundaries. Vanadium (VC) and chromium (Cr_7C_3) carbides are respectively observed in AISI O2 (Fig. 2, *a*) and AISI D2 (Fig. 2, *b*)

steels along with the iron (Fe_3C) and complex $(V,Fe)C$, $(Cr,Fe)_7C_3$) carbides. XRD data confirmed the existence of VC and Cr_7C_3 carbides and refined ferrite crystallites (manifested as the broadened diffraction peaks). The afore-referred works [14, 51, 52] also revealed the physical nature of significant and stable hardening. Several microstructural features of the LHT + UIT processed layers were concluded to provide the stability of their microstructure. They were the following: an ultra-fine grained structure, the high density of dislocations and their bundles in the grain/subgrain volume, and fine carbides (Cr_7C_3, $(Cr,Fe)_7C_3$) fixed both the dislocations and grain/subgrain boundaries and prevented slipping along the grain/subgrain boundaries at the applied mechanical and/or thermal loads [14, 52]. This microstructural analysis correlates well to other literature works reported on the grain refinement and enhanced mechanical properties of tool steels modified by laser surface hardening [33, 41–43], laser surface melting/alloying [32, 39] and/or SMAT [8, 35].

In some experiments, the surface layers hardened by a single UIT process demonstrated the increase in hardness, but the decreased wear resistance at friction tests was simultaneously observed for these surface layers [14]. The authors associated that result with the fact that the dislocation structure formed at UIT had insufficient stability because it was supposedly produced only by strain in one direction and fixed by elastic stresses and could be relatively easily rearranged during the friction process. When such structures are subjected to periodical loads at friction, there is a peculiar manifestation of the Bauschinger effect [56], in which the predeformation in one direction facilitates subsequent deformation in other directions. Such an effect is of scientific interest, however, the layers hardened in this way cannot be used to establish the general regularities of the friction wear rate.

4.2. Mechanical and Tribological Properties of Steels in the Initial State and Hardened Surface Layers

The experimentally obtained mechanical and tribological properties of studied samples are given in Table 2. The obtained dataset is an example of the possibilities of the new methodology for characterization of the hardening extent and friction wear of the hardened surface layers.

It can be seen from the results presented in Table 2 that the actual hardening extent of the surface, which is determined by accounting the yield stress σ_S, is significantly greater than the hardening extent assessed on the base of the increase in the hardness value.

For the hardened state of the surface layer of the AISI O2 steel, the hardening extents became respectively equal to 3.45 and 5.98 when they were assessed according to the measured hardness and the evaluated
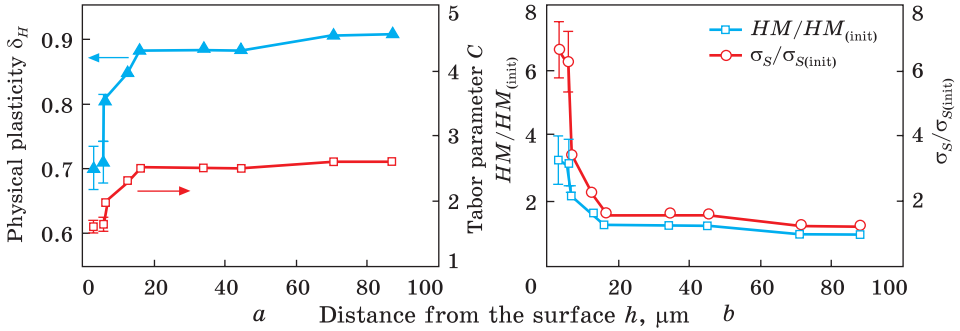
Fig. 3. Dependences of physical plasticity δ_H and Tabor parameter C (*a*), and the hardness ratio, $HM/HM_{(init)}$ and the yield stress ratio $\sigma_S/\sigma_{S(init)}$ (*b*) on the distance h from the hardened surface of the AISI O2 steel sample. The subscript 'init' indicates the initial state

Table 2. **Mechanical properties of the surface layers and characteristics of the friction wear of the investigated steels (here, *HM* is the Meyer hardness, δ_H is the physical plasticity, *C* is the Tabor parameter, σ_S is the yield stress, *W* is the depth of the friction wear groove, K_f is the friction plasticity coefficient, and *WR* is the relative wear rate)**

Material	State	HM, GPa	δ_H	C	σ_S, GPa	$\dfrac{HM}{HM_{(init)}}$, Pa	$\dfrac{\sigma_S}{\sigma_{S(init)}}$	W, μm	K_f	WR
AISI O2	Initial	2.56	0.95	3.24	0.79	1.00	1.00	5.33	0.48	1.00
	Hardened	8.86	0.77	1.87	4.73	3.45	5.98	0.57	0.33	0.11
AISI D2	Initial	3.00	0.88	2.45	1.22	1.00	1.00	3.40	0.43	0.64
	Hardened	5.30	0.80	2.00	2.86	1.76	2.30	1.29	0.35	0.24

yield stress. Therefore, for the essentially hardened surface layers, an evaluation of the hardening extent on the base of the hardness magnitude appears significantly underrated.

We explain such a difference by the fact that an increase in the yield stress σ_S would naturally result in the material plasticity (including physical plasticity δ_H) diminution, which, in turn, would cause a decrease in the Tabor parameter C (see Fig. 1). Therefore, following Eq. (2), the Meyer hardness HM would be grown less than the yield stress σ_S. This observation indicates that the hardening extent of the surface layers can be better characterized by the yield stress σ_S rather than by the hardness.

Analysis of the results listed in Table 2 also shows that the increase of hardness and yield stress of the surface layer is accompanied by the decrease of physical plasticity δ_H. Moreover, for substantially hardened surface layers the δ_H may become lesser than the critical value $\delta_{H_c} \approx 0.9$, below which the bulk materials undergoing the tensile test lose their

plasticity. However, the value of physical plasticity δ_H of the surface layers of the steel samples investigated in this article (see Table 2) appears to be still quite sufficient for the prevention of the destruction of thin surface layers [57].

Additionally, the application of the indentation method allows revealing a gradient character of the changes in the mechanical properties of the hardened layers depending on the distance from the treated surface (Fig. 3). The surface layers with gradient microstructure and mechanical properties are known can be formed on the tool (ferritic) steels [14, 33, 35, 39, 42, 43, 51], austenitic steels [15, 38, 41] and other metallic alloys based on Cu [36, 58, 59], Al [40]. To determine the yield stress σ_S and the Tabor parameter C on the base of the measured hardness, the above-described simplified methodology and Fig. 1 have been respectively used.

Figure 3 shows the experimental data describing gradual changes in mechanical properties of the surface layer of the hardened AISI O2 steel sample. Rational dependencies of the acquired hardness HM and yield stress σ_S are shown with respect to the hardness $HM_{(init)}$ and yield stress $\sigma_{S(init)}$ of the initial samples of AISI O2 steel. Additionally, the depth dependences of the Tabor's parameter C and plasticity characteristic δ_H are also presented. It is seen that the hardened layer possessing very high yield stress, is rather thin, and the yield stress sharply decreases from the outmost to the deeper ones down to the initial yield stress of the sample core.

Moreover, it is evident from Fig. 3 that not only the values of the yield stress σ_S and physical plasticity δ_H are gradually changing (σ_S increases and δ_H decreases) while the examined near-surface layer becomes closer to the hardened surface of the sample, but also the magnitude of the Tabor's parameter C is decreasing in the layers located closer to the sample surface.

Figure 3 confirms the expediency of characterizing the strength of the hardened layer by the generally accepted strength characteristic — the yield stress — but not by the hardness. The physical plasticity δ_H of the hardened layer is also of interest to characterize the friction wear of the material (see next section).

4.3. Wear Rate Assessment Using a New Methodology

For analysis of the wear process and assessment of the wear rate, the hardness value is widely used (see, *e.g.*, Refs. [8, 14, 16, 60]). However, the results obtained in [29] show that the hardness magnitude characterizes the stress, which should be applied to the indenter to provide its penetration into the material. Further, as can be seen from Eq. (1), the Meyer hardness HM exceeds the yield stress σ_S of the material. Moreover, this excess, which is characterized by the Tabor's parameter C,

can vary in a wide interval. Indeed, the Tabor parameter C magnitude may range from 4 for pure aluminium to 1 for ceramics (Fig. 1). Moreover, C depends on the structure of a material.

Accounting the fact that the stress field occurring at the friction process is substantially different from that forming by the indenter at the hardness measurement, we think that to describe the wear rate it is more expedient to use the values of the yield stress σ_S and the physical plasticity δ_H. The wear rate of material assessed on the base of its hardness appears inaccurate.

### 4.3.1. A Generalized Scheme for the Dependence of Wear Rate on the Physical Plasticity δ_H

Data available in the literature give grounds to assume that the influence of δ_H on the wear rate can be different in the wear process induced by plastic deformation [14, 29] and in the wear process, which is caused by the brittle fracture leading to the chipping and removal of material particles [27].

It was shown in [37] that a better correlation of experimental and calculated dependences of the wear resistance W^{-1} on hardness can be obtained when the Archard–Rabinowicz formula (for steels) [8, 11, 14, 60] contains the HM/δ_H ratio, but not the HM hardness value itself. It was also shown that the δ_H increase would result in the reduction of the wear resistance (*i.e.*, the wear rate increase) when the plastic deformation would be the main wear mechanism. The same results are obtained in this study (see Table 2).

At the same time, when the tool made of the hard alloy was used for stamping high-strength steel [27], the wear rate of the tool was observed to be increased (*i.e.*, the wear resistance decreased) with decreasing physical plasticity δ_H. In Ref. [27], the relative wear rate WR was given only for the hard alloys. For the reason of reliable comparison, we have calculated WR for the investigated steels as well (see Table 2). Similar to [27], the wear rate was taken to be equal to one ($WR = 1$) for the material with the highest wear rate (steel AISI O2 in the initial state). The generalized scheme of the δ_H influence on the relative wear rate WR is constructed on the base of experimental results obtained in this study for steels and using literature data for hard alloys [27] (Fig. 4). It is seen that the curve $WR = f(\delta_H)$ has a minimum at $\delta_H \approx 0.77$.

The δ_H for hard alloys is naturally much lower ($\delta_H \approx 0.67{-}0.77$) than those for steels, and their wear rate increases with decreasing δ_H. Therefore, the wear rate of hard alloys is caused by a fracture and removal of the particles detached from their surfaces. Conversely, the wear rate of steels increases with increasing physical plasticity δ_H as it is caused by plastic deformation.

Fig. 4. Dependence of relative wear rate *WR* on physical plasticity δ_H. '*A*' and '*B*' indicate the regions, where the fracture (*A*) and plastic deformation (*B*) are the dominant mechanisms of wear. Circles correspond to data for hard alloys [27], and squares (*1*−*4*) show the data for the initial (*1*, *2*) and hardened (*3*, *4*) samples of AISI O2 (*1*, *4*) and AISI D2 (*2*, *3*) steels
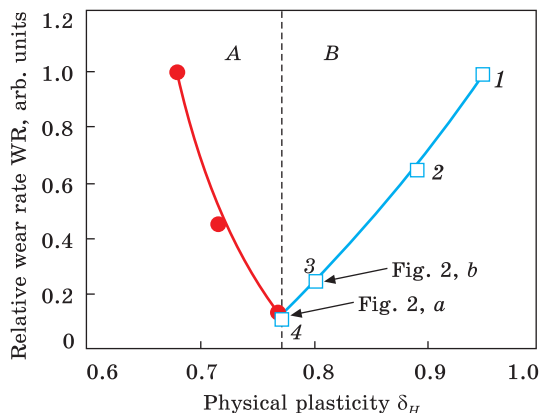
It is of essential interest that the significantly hardened layer of the AISI O2 steel (Table 2) underwent very weak wear (*W* = 0.57 μm and *WR* = 0.11), and is characterized by low friction plasticity coefficient K_f = 0.33, *i.e.* the pile-ups along the wear groove sides are very small. For this layer, the physical plasticity δ_H is equal to 0.77. Such plasticity is low for the wear caused by plastic deformation. However, it is large enough to provide a significant reduction in the wear induced by fracture of hard alloys. This conception is confirmed by Fig. 4, which shows that the wear rate of the hard alloy (characterized by δ_H = 0.77) is substantially reduced in comparison with the other hard alloys possessing lower physical plasticity.

Thus, we can assume that there is an optimal magnitude of physical plasticity $\delta_H \approx 0.77$, which provides a very small wear rate caused both by plastic deformation and by fracture. At the value of physical plasticity δ_H = 0.77, the wear caused by plastic deformation is sharply reduced due to the low plasticity of the material, and the wear caused by brittle fracture is simultaneously reduced because this δ_H magnitude is higher than the δ_H value triggering the brittle fracture process.

To show the applicability of the proposed methodology for a wider range of materials, we also studied the wear behaviour of the (111) plane of single-crystalline silicon (using the same wear test conditions as those used in the case of steel samples). It should be noted that for ceramic materials and covalent crystals, where physical plasticity decreases to very small values (δ_H = 0.4−0.5), the wear rate is expected to be much higher than that for hard alloys shown in Fig. 4. Experimental results obtained for the Si sample (δ_H = 0.4) show that the worn groove observed was characterized by a very high depth (*W* = 26 μm).

Consequently, for the materials, which possess a lower physical plasticity δ_H than those for the hard alloys, the wear rates *WR* in the brittle fracture region ('*A*' region in Fig. 4) are shown to be increased.

The shown in Fig. 4 scheme can be used to select a material that would demonstrate a low wear rate or would possess an optimal combination of such characteristics as the yield strength, physical plasticity, and wear rate.

The LHT + UIT process respectively results in an about triple and ten-time decrease in the wear rate (*W*) of AISI D2 and AISI O2 steel samples. The observed difference in the wear resistance increase for the studied steels correlates well to the difference in their hardening ability (see Table 2) and can be explained by the peculiarities of their microstructure in the initial and hardened states. Indeed, the initial samples of AISI D2 steel contain relatively coarse Cr_7C_3 carbide particles/plates [14, 52], and this steel, therefore, is less prone to both the thermal and strain hardening at the LHT + UIT process. On the contrary, the initial AISI O2 steel samples with ferritic-pearlitic structure and dispersed primary VC carbides demonstrate a higher ability to the laser transformation hardening, which is brought about by the formation of finest martensitic grains with fine secondary VC carbides, and to further strain hardening (at UIT) occurred owing to the grain/subgrain refinement.

Nevertheless, the enhanced wear resistance of both steels is vitally related to the formation of the surface layer hardened owing to complex thermal (LHT) and mechanical (UIT) process. Rapid thermal treatment by a laser beam (heating followed by quenching) forms the fine martensitic structure, supports the solid solution hardening due to dissolution of primary vanadium and chromium carbides, and dispersion hardening by precipitation of fine secondary VC (Fig. 2, *a*) and $(CrFe)_7C_3$ (Fig. 2, *b*) carbides. Further severe plastic deformation by UIT results in dislocation multiplications and rearrangements and formation of cell dislocation structure (Fig. 2). Moreover, both the separate dislocations and the cell/grain boundaries are effectively blocked by secondary carbides, which support the grain boundary hardening and enhance their firmness and stability of the formed microstructure at the friction process.

4.3.2. An Equation Describing the Effect of Yield Stress σ_S and Physical Plasticity δ_H on the Plastic-Deformation-Caused Wear Rate W

The results of the previous sections demonstrate that the wear caused by plastic deformation grows with increasing δ_H. We will assume that in this case, *W* is proportional to δ_H, since the higher the δ_H, the greater the plastic deformation of the sample. Data shown in Fig. 4 correspond to such regularity.

To construct an analytical expression for the dependence $W = f(\delta_H, \sigma_S)$ we must take into account that the wear caused by plastic deformation is generally lower for the materials possessing higher hardness. Usually, the wear loss is considered approximately inversely proportional to hardness *H* of material [8, 14, 60]. But taking into

Fig. 5. Dependence of the wear rate *W* of the investigated AISI O2 (*1*, *4*) and AISI D2 (*2*, *3*) steels on their δ_H/σ_S ratios in the initial (*1*, *2*) and hardened (*3*, *4*) states
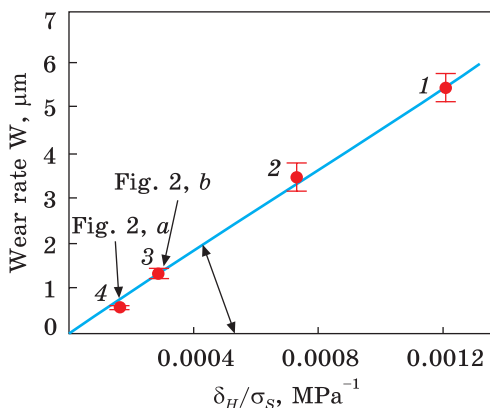
account the above-given discussion we see that to express the resistance of the material to plastic deformation during the wear process the yield stress σ_S is much better (and accurate) characteristic than the hardness magnitude *H*.

Thus, considering above-listed observations the following expression can be proposed for the description of the $W(\delta_H, \sigma_S)$ dependence if the wear would be caused by plastic deformation:

$$W = N\delta_H/\sigma_S, \qquad (6)$$

where N = const, which depends on the tribology method that was used to wear rate determination.

Obtained results in coordinates of Eq. (6) are plotted in **Fig. 5**. It is seen that the obtained data stand to a straight line indicating that they are satisfactorily described by the relation (6) with $N \approx 4.44$ GPa·µm.

The known physical concepts of the wear mechanism during friction do not allow us to perform a theoretical calculation of the N value.
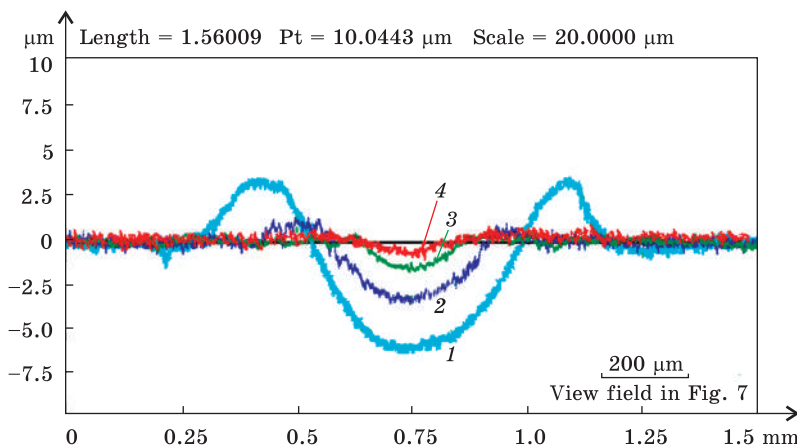

Fig. 6. Wear track profiles of the AISI O2 (*1*, *4*) and AISI D2 (*2*, *3*) steels in the initial (*1*, *2*) and hardened (*3*, *4*) states. Horizontal marker indicates the area of the view field in the SEM images presented in the next figure

Thus, the N magnitude was determined experimentally from the slope of the straight line in the graph W *vs.* (δ_H/σ_S) (tan α in Fig. 5).
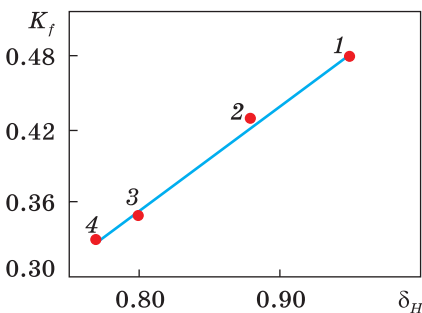
Structural parameters of material, such as grain size, dislocation density, dispersed particles of the second phase, *etc.*, exert their influence on σ_S and δ_H, and they are therefore taken into account in Eq. (6).

While constructing the $W(\delta_H/\sigma_S)$ dependence, it was taken into account that plastic deformation is absent at $\delta_H = 0$, and therefore, the wear, induced by plastic deformation, must be absent as well ($W = 0$). With such an assumption, the straight line in Fig. 6 should pass through the origin, and this is observed.

The aim of further works, which are in progress now, consists of clarifying the applicability of the proposed Eq. (6) for a satisfactory description of numerous experimental data available in the literature concerning the wear rate of other steels and metallic alloys induced by plastic deformation. The dependence of the constant N on the tribological conditions for the wear-rate determination method has to be investigated as well.

4.3.3. Peculiarities of the Wear Track Profiles and Worn Surfaces

The $W = f(\delta_H)$ scheme (Fig. 4) and dependence $W = f(\delta_H/\sigma_S)$ (Fig. 5) become clearer with analysing the wear track profiles and morphologies of the worn surfaces. Figure 6 demonstrates cross-sections of the wear tracks of the samples studied, and the morphology of the worn surfaces is shown in Fig. 7. The highest wear losses (the worn track depths) are seen for both initial samples. Both the untreated steel samples are characterized with marked pile-ups alongside the wear tracks and longitudinal slip lines on the wear track bottom. This confirms that the wear is predominantly governed by plastic deformation mechanisms ('ploughing' and/or pile-ups forming). It is confirmed by the values of the physical plasticity δ_H (respectively 0.95 and 0.88 in Table 2) and friction plasticity parameters K_f (0.48 and 0.43) respectively assessed using Eqs. (1) and (5). The main operative microstructural constituents providing the load-bearing capacity of both steels in the initial state are pearlitic grains. The higher volume fraction of ferritic grains in AISI O2 steel provides easier plastic deformation during the friction process. At the same time, the higher volume fraction of primary $(CrFe)_7C_3$ carbides in

Fig. 7. Relation between the friction plasticity coefficient K_f and the physical plasticity δ_H for the investigated AISI O2 (*1*, *4*) and AISI D2 (*2*, *3*) steels

the AISI D2 steel sample results in higher HV, essentially higher σ_S (Table 2), slightly lower physical plasticity δ_H, and better anti-wear performance.

Another situation is observed after complex hardening processing. The wear track profiles of the LHT + UIT processed samples (indicated by points *3* and *4* in Figs. 4–7) demonstrate much lower wear track depths and negligible heights of the pile-ups formed. It witnesses that plastic deformation is essentially limited due to LHT + UIT hardening of the sample surfaces (δ_H became 0.77 and 0.8 and K_f became 0.35 and 0.33 for AISI D2 and AISI O2 steels, respectively, samples *3* and *4* in Figs. 4–7).

It is important that friction plasticity coefficient K_f correlates with the physical plasticity δ_H for investigated steels, and this correlation is close to the linear proportionality (Fig. 7). The K_f value can be evaluated for investigated steels by the following equation:

$$K_f = 0.86\,\delta_H - 0.33. \tag{7}$$

Naturally, such dependence can be used only for the sufficiently ductile materials, the wear of which is accompanied by the appearance of the wedge and/or pile-ups. For such materials, the physical plasticity reads $\delta_H \geq 0.75$.

The observed clear correlation of friction plasticity coefficient K_f suggested in [53] and the physical plasticity δ_H confirms that the coefficient K_f assessed on the base of the analysis of the wear track shape can be used as a characteristic for the plasticity of metallic alloys.

The SEM observations (Fig. 8) were utilized to complement the profilometry data of the worn tracks. Typical SEM micrographs of the studied worn surfaces allow elucidating the modes of wear loss in the studied cases; the sliding direction is vertical (along the wear groove) in all the images. However, the length of the slip lines decreases at the decrease of physical plasticity δ_H for steels in the initial state. The presence of continuous grooves along the sliding direction points to extensive plastic deformation (Figs. 8, *a*1 and *b*2). The grooved morphology indicates the same 'ploughing' wear mechanism of both the initial steels throughout the process. It can be seen, however, that more rarely grooves were formed in the initial AISI D2 steel sample (Fig. 8, *b*2).

On the contrary, the worn surfaces of the LHT + UIT processed samples contain short slip lines, which appear mainly along the wear groove but some groups of the slip lines are arbitrarily directed especially in the hardened AISI O2 steel (Fig. 8, *d*4). The formation of such groups of slip lines occurs owing to the delamination of fine particles by ductile fracture. Thus, the wear process of significantly hardened surface layers occurs both by the 'ploughing' and by the removal of particles chipped away by ductile fracture. Microcracks that usually appear during brittle
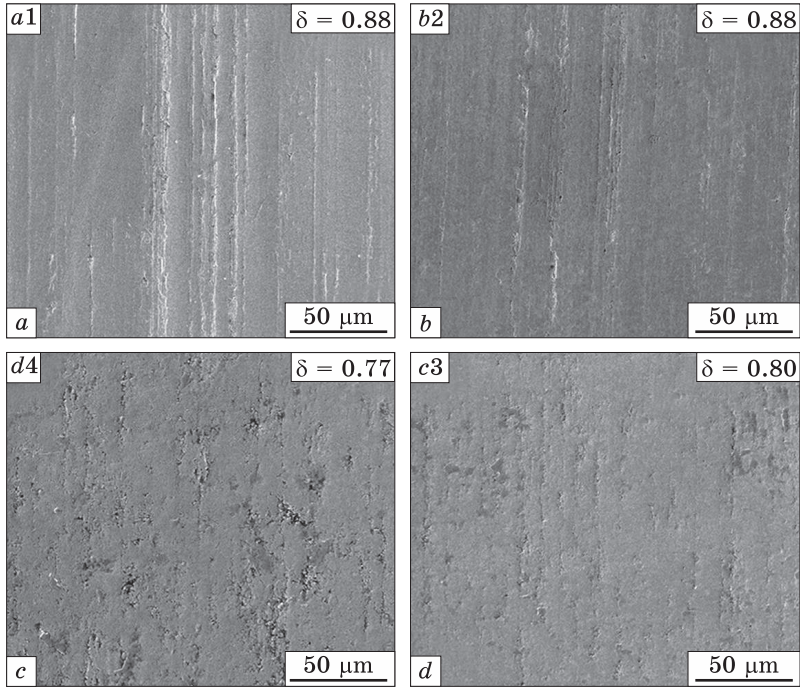
Fig. 8. SEM observations of the wear tracks on the AISI O2 (*a*1, *d*4) and AISI D2 (*b*2, *c*3) steels in the initial (*a*1, *b*2) and hardened (*c*3, *d*4) states. Numerals (*1*−*4*) correspond to the states shown in Figs. 4−6

and quasi-brittle fracture are not detected in Fig. 8. Notice that both the wear mechanisms operated in the hardened layers provide a very low wear rate. The worn surfaces are smooth and almost damage-free owing to the high hardening extent achieved (Figs. 8, *c*3 and *d*4). Wear track is evidently more homogeneous for AISI D2 steel samples (Fig. 8, *c*3) than that for AISI O2 steel samples (Fig. 8, *d*4). It can be explained by the TEM observations indicated that after the LHT + UIT process the secondary VC carbides precipitated in the fine martensitic structure of AISI O2 steel (Fig. 2, *a*) are finer and more homogeneously distributed than the $(CrFe)_7C_3$ carbides in AISI D2 steel (Fig. 2, *b*). However, a high hardening extent is accompanied by the lowered plasticity, which appears to facilitate the pullout and removal of grain fragments or carbide particles, and somewhere results in the formation of the dark areas (cavities). The enhanced wear resistance of these samples brings about the optimal magnitude of physical plasticity δ_H. It is too low to promote the intensive wear caused by plastic deformation and it is simultaneously too high to allow the intensive wear caused by the brittle or quasi-brittle fracture process.

An essential question is: could the wear of AISI O2 steel be further lowered by more intensive hardening and accompanied decrease in its

physical plasticity δ_H? The direct answer can be found in Fig. 4: further decrease in δ_H results in the transition of this steel to the '*A*' area, in which the main wear mechanism of the material is fracture and removal of the worn particles. The particle delamination can occur by either quasi-brittle fracture or even the brittle fracture accompanied by microcracks formation and essential loss in the strength of the hardened layer. In this case, the wear rate should be increased according to Fig. 4. Therefore, we can conclude that the condition $\alpha_H \geq 0.77$ should be met for the hardened layers of steel sample, and the values of physical plasticity δ_H ranged within $0.77–0.80$ can be accepted to be optimal. Such value was achieved by the combined laser heat treatment and ultrasonic impact treatment in this work.

4.3.4. Algorithm for the Wear Rate Estimation

The methodology of the application of the yield stress σ_S and physical plasticity δ_H determined by the indentation methods suggested in this paper for characterization of the friction wear and hardening extent of the surface layers/coatings can be described using the algorithm presented in Fig. 9. This algorithm defines the sequence of experimental measurements using the indentation method and theoretical evaluations using several equations reported in the paper, which are required to be performed to obtain the wear rate values for the studied surface layers (or coating).

Regardless of the hardening method used, the samples for the indentation tests should be first prepared. Then, the hardness and elastic
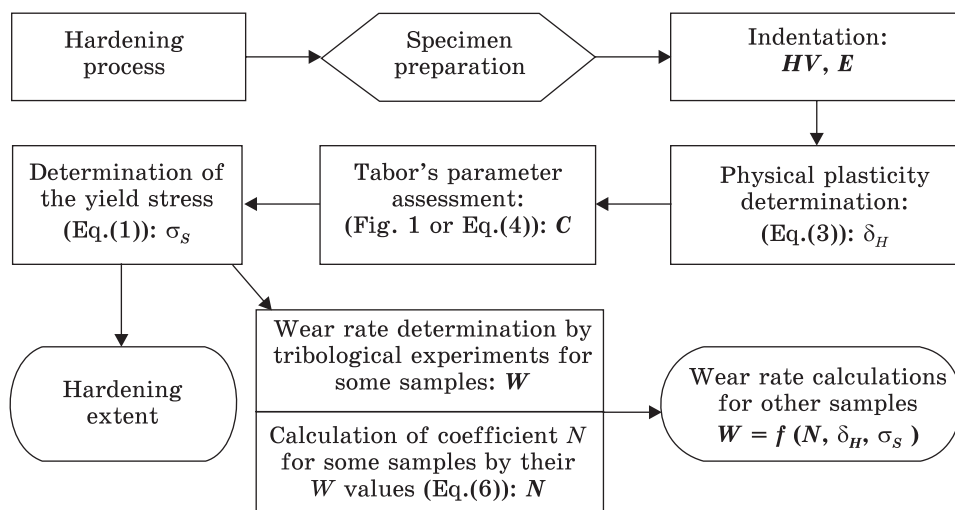

Fig. 9. Algorithm defining the operations' sequence for the hardening extent and wear rate assessments using mechanical properties of the surface layers as determined by indentation

modulus magnitudes should be measured. For standard steels, the reference values of elastic modulus are available and can be easily used.

After that, the physical plasticity δ_H can be evaluated using Eq. (3), and the Tabor's parameter C can be assessed using Fig. 1 or Eq. (4). The yield stress σ_S of the hardened surface layer can then be determined from the Tabor equation for Meyer hardness (Eq. (1), but with $C = f(\delta_H)$ in this case).

The wear rate for some samples should be determined experimentally using, for example, the techniques described in section 3.4. Further, the parameter N in Eq. (6) should be assessed as $\tan\alpha$ in Fig. 5. Then, the wear rate for other samples could be evaluated using Eq. (6), if their δ_H and σ_S values would be determined. It should be taken into account that the parameter N depends on the tribological conditions of the wear tests.

In such a way, the suggested methodology described by the proposed algorithm can be applied to replace a part of time-consumable wear experiments.

5. Conclusions

For a mathematical description of the wear process of metal alloys during friction, it is necessary to use the plasticity characteristic of the material, since plastic deformation plays a decisive role in the wear mechanism of these alloys. However, the widely used plasticity characteristic, namely, elongation to fracture in a tensile test, δ, cannot be used for this purpose. Firstly, δ does not correspond to the modern definition of plasticity, and, secondly, this characteristic cannot be determined for thin surface layers and coatings contacting with the counter-body. It is proposed in the article to use the physical plasticity δ_H to describe the wear process. The physical plasticity δ_H was earlier introduced by the authors of Ref. [28] and successfully used for other applications; it corresponds to the physical definition of plasticity and can be determined by micro- or nanoindentation methods.

To characterize the strength of material during friction wear, the hardness value is usually used, justifying this by the fact that the Meyer hardness HM is proportional to the yield stress σ_S following the Tabor's equation $HM = C\sigma_S$ at $C = \text{const}$. The authors showed that C depends on the structural state of the material and it decreases with the material hardening. Therefore, when studying the process of wear during friction, it is advisable to characterize the strength using the yield stress σ_S, but not the HM value. A simple method for determining the Tabor's parameter C using Eq. (4) or using Fig. 1 is proposed. After that, the yield stress σ_S can be calculated according to the above Tabor's equation.

The suggested formula for the dependence of the wear rate W caused by plastic deformation on the yield stress σ_S and physical plasticity δ_H ($W = N\delta_H/\sigma_S$ at $N = $ const) satisfactorily describes the experimentally registered wear data for the steels studied in the initial state and after hardening by the combined laser heat treatment and ultrasonic impact treatment.

The generalized scheme of the dependence of wear rate W of the material on its physical plasticity δ_H is proposed. The $W = f(\delta_H)$ is based on considering the experimentally obtained results for the AISI O2 and AISI D2 steel samples and literature data for hard alloys. The dependence $W(\delta_H)$ goes through the minimum at $\delta_H \approx 0.77$. For the studied steel samples, the inequality $\delta_{H\min} \leq \delta_H < 1$ is true and the wear rate W increases with increasing δ_H indicating that the main wear mechanism is the plastic deformation. Conversely, for hard alloys, the inequality $0.67 < \delta_H \leq \delta_{H\min}$ is true and the wear rate W decreases with increasing δ_H, which conforms to the idea that the main wear mechanism of these materials is fracture and removal of the worn particles. The obtained results suggest that, while the hardening extent of the steel surface layer becoming larger, the physical plasticity δ_H is getting lower, and for $\delta_H < 0.77$, the main wear mechanism should be changed to the surface fracture that would increase the wear rate.

For the hardened surface layers of the steel samples, optimal values of physical plasticity δ_H are $0.77-0.80$. At such δ_H values, very low wear rate, increased yield stress, and hardness are observed, and plasticity is sufficient for the operation under extreme conditions without fracture. In this work, thin surface layers possessing such mechanical properties were produced by the combined laser heat treatment and ultrasonic impact treatment.

REFERENCES

1. E. Rabinowicz, *Friction and Wear of Materials* (Wiley: New York: 1995).
2. I.V. Kragelsky, *Tribology: Lubrication, Friction and Wear* (John Wiley and Sons Ltd: Bury St Edmunds: 2005).
3. I.M. Lyubarskyi and L.S. Palatnik, *Metallofizika Treniya* [Metal Physics of Friction] (Moscow: Metallurgy: 1976) (in Russian).
4. A.R. Chintha, *Mater. Sci. Technol.*, **35**, No. 10: 1133 (2019).
   https://doi.org/10.1080/02670836.2019.1615669
5. H.K.D.H. Bhadeshia, *Prog. Mater. Sci.*, **57**, No. 2: 268 (2012).
   https://doi.org/10.1016/j.pmatsci.2011.06.002

6. J.D. Lemm, A.R. Warmuth, S.R. Pearson, and P.H. Shipway, *Tribology Int.*, **81**: 258 (2015).
   https://doi.org/10.1016/j.triboint.2014.09.003

7. Y. Zhu, W. Wang, R. Lewis, W. Yan, S. R. Lewis, and H. Ding, *J. Tribol.*, **141**, No. 12: 120801 (2019).
   https://doi.org/10.1115/1.4044464

8. L. Zhou, G. Liu, Z. Han and K. Lu, *Scr. Mater.*, **58**, No. 6: 445 (2008).
   https://doi.org/10.1016/j.scriptamat.2007.10.034

9. K. Kato, *Proc. Inst. Mech. Eng. Part J: J. Eng. Tribology*, **216**, No. 6: 349 (2002).
   https://doi.org/10.1243/135065002762355280

10. M.F. Ashby and S.C. Lim, *Scr. Met. Mater.*, **24**: 805 (1990).
    https://doi.org/10.1016/0956-716X(90)90116-X.

11. S.A. Bespalov, *Usp. Fiz. Met.*, **10**, No. 4: 415 (2009) (in Russian).
    https://doi.org/10.15407/ufm.10.04.415

12. A. Jafari, K. Dehghani, K. Bahaaddini, and R. A. Hataie, *Wear*, **416−417**: 14 (2018).
    https://doi.org/10.1016/j.wear.2018.09.010

13. H. de Beure and J.Th.M. de Hosson, *Scr. Metal.*, **21**, No. 5: 627 (1987).
    https://doi.org/10.1016/0036-9748(87)90373-5

14. D.A. Lesyk, S. Martinez, B.N. Mordyuk, V.V. Dzhemelinskyi, A. Lamikiz, G.I. Prokopenko, Yu.V. Milman, and K.E. Grinkevych, *Surf. Coat. Technol.*, **328**: 344 (2017).
    https://doi.org/10.1016/j.surfcoat.2017.08.045

15. S.I. Sidorenko, M.O. Vasylyev, and S.M. Voloshko, *Materials Science: Achievements and Prospects* (Eds. L.M. Lobanov et al.) (Kyiv: Akademperiodyka: 2018), p. 393 (in Ukrainian).
    http://u-i-n.com.ua/en/catalog_main/203

16. M.O. Vasiliev, G.I. Prokopenko, and V.S. Filatova, *Usp. Fiz. Met.*, **5**, No. 3: 345 (2009) (in Russian).
    https://doi.org/10.15407/ufm.05.03.345

17. B.N. Mordyuk, M.O. Iefimov, Yu.V. Milman, G.I. Prokopenko, V.V. Silbershmidt, M.I. Danylenko, and A.V. Kotko, *Surf. Coat. Technol.*, **202**, No. 19: 4875 (2008).
    https://doi.org/10.1016/j.surfcoat.2008.04.080

18. Yu.V. Milman, K. Grinkevich, S. Chugunova, W. Lojkowski, M. Djahanbakhsh, and H.J. Fecht, *Wear*, **258**, Nos. 1−4: 77 (2005).
    https://doi.org/10.1016/j.wear.2004.02.017

19. E.M. Rudenko, V.Ye. Panarin, P.O. Kyrychok, M.Ye. Svavilnyi, I.V. Korotash, O.O. Palyukh, D.Yu. Polotskyi, and R.L. Trishchuk, *Prog. Phys. Met.*, **20**, No. 3: 485 (2019).
    https://doi.org/10.15407/ufm.20.03.485

20. J. W. Murray, N. Ahmed, T. Yuzawa, T. Nakagawa, S. Sarugaku, D. Saito, and A.T. Clare, *Tribology Int.*, **150**: 106392 (2020)
    https://doi.org/10.1016/j.triboint.2020.106392

21. O.V. Maksakova, O.D. Pogrebnjak, and V.M. Beresnev, *Prog. Phys. Met.*, **19**, No. 1: 25 (2018).
    https://doi.org/10.15407/ufm.19.01.025

22. M.A. Vasylyev, B.N. Mordyuk, S.I. Sidorenko, S.M. Voloshko, A.P. Burmak, I.O. Kruhlov, and V.I. Zakiev, *Surf. Coat. Technol.*, **361**: 413 (2019)
    https://doi.org/10.1016/j.surfcoat.2018.12.010

23. B.N. Mordyuk, G.I. Prokopenko, K.E. Grinkevych, N.A. Piskun, and T.V. Popova, *Surf. Coat. Technol.*, **309**: 969 (2017).
    https://doi.org/10.1016/j.surfcoat.2016.10.050

24. Yu.V. Milman, S.I. Chugunova, I.V. Goncharova, and A.A. Golubenko, *Prog. Phys. Met.*, **19**, No. 3: 271 (2018).
https://doi.org/10.15407/ufm.19.03.271

25. A.F. Shchurov, A.V. Kruglov, and V.A. Perevoshchikov, *Inorg. Mater.*, **37**, No. 4: 349 (2001).
https://doi.org/10.1023/A:1017571609977

26. P.H. Boldt, G.C. Weatherly, and J.D. Embury, *Int. J. Mater. Res.*, **15**, No. 4: 1025 (2000).
https://doi.org/10.1557/JMR.2000.0146

27. X. Zhang, B.D. Beake, and S. Zhang, *Thin Films and Coatings. Toughening and Toughness Characterization* (Ed. S. Zhang) (Boca Raton: Taylor & Francis Group, CRC Press: 2015), Ch. 2, p. 48.
https://doi.org/10.1201/b18729

28. Yu.V. Milman, B.A. Galanov, and S.I. Chugunova, *Acta Met. Mater.*, **41**, No. 9: 2523 (1993).
https://doi.org/10.1016/0956-7151(93)90122-9

29. B.A. Galanov, Yu.V. Milman, S.I. Chugunova, I.V. Goncharova, and I.V. Voskoboinik, *Crystals*, **7**, No. 3: 87 (2017).
https://doi.org/10.3390/cryst7030087

30. Yu.V. Milman, *J. Phys. D: Appl. Phys.*, **41**: 074013 (2008).
https://doi.org/10.1088/0022-3727/41/7/074013

31. M.J. Schneider and M.S. Chatterjee, *ASM Handbook. Vol. 4A. Steel Heat Treating Fundamentals and Processes* (Eds. J. Dossett and G.E. Totten) (ASM International: 2013), p. 389.

32. J. Grum, *J. Ach. Mater. Manuf. Eng.*, **24**, No. 1: 17 (2007).
http://jamme.acmsse.h2.pl/papers_vol24_1/24101.pdf

33. Y. Morisada, H. Fujii, T. Mizuno, G. Abe, T. Nagaoka, and M. Fukusumi, *Mater. Sci. Eng. A*, **505**, Nos. 1–2: 157 (2009).
https://doi.org/10.1016/j.msea.2008.11.006

34. A.L. Ortiz, J.-W. Tian, L.L. Shaw, and P.K. Liaw, *Scr. Mater.*, **62**, No. 3: 129 (2010).
https://doi.org/10.1016/j.scriptamat.2009.10.015

35. S. Lu, Z. Wang, and K. Lu, *J. Mater. Sci. Technol.*, **26**, No. 3: 258 (2010).
https://doi.org/10.1016/S1005-0302(10)60043-6

36. A. Amanov, I.-S. Cho, and D.-E. Kim, *Mater. Design*, **45**: 118 (2013).
https://doi.org/10.1016/j.matdes.2012.08.073

37. L. Li, M. Kim, S. Lee, M. Bae, and D. Lee, *Surf. Coat. Technol.*, **307**: 517 (2016).
https://doi.org/10.1016/j.surfcoat.2016.09.023

38. C. Ye, A. Telang, A.S. Gill, S. Suslov, Y. Idell, K. Zweiacker, J.M.K. Wiezorek, Z. Zhou, D. Qian, S.R, Mannava, and V.K. Vasudevan, *Mater. Sci. Eng. A*, **613**: 274 (2014).
https://doi.org/10.1016/j.msea.2014.06.114

39. T. Amine, J.W. Newkirk, H. El-Din, F. El-Sheikh, and F. Liou, *Int. J. Adv. Manuf. Technol.*, **73**: 1427 (2014).
https://doi.org/10.1007/s00170-014-5882-8

40. U. Trdan, M. Skarba, J.A. Porro, J.L. Ocana, and J. Grum, *Surf. Coat. Technol.*, **342**: 1 (2018).
https://doi.org/10.1016/j.surfcoat.2018.02.084

41. J. Radziejewska, *Mater. Design*, **32**, No. 10: 5073 (2011).
https://doi.org/10.1016/j.matdes.2011.06.035

42. J.H. Lee, J.H. Jang, B.D. Joo, Y.M. Son, and Y.H. Moon, *Trans. Nonferrous Met. Soc. China*, **19**, No. 4: 917 (2009).
https://doi.org/10.1016/S1003-6326(08)60377-5

43. G. Telasang, J.D. Majumdar, G. Padmanabham, and I. Manna, *Surf. Coat. Technol.*, **261**: 69 (2015).
https://doi.org/10.1016/j.surfcoat.2014.11.058

44. D. Tabor, *Phil. Mag. A*, **74**, No. 5: 1207 (1996).
https://doi.org/10.1080/01418619608239720

45. Y.T. Cheng and C.M. Cheng, *Mater. Sci. Eng. R*, **44**, No. 4: 91 (2004).
https://doi.org/10.1016/j.mser.2004.05.001

46. Y. Milman, S. Dub, and A. Golubenko, *MRS Proceedings*, **1049**: 1049-AA05-06 (2007).
https://doi.org/10.1557/PROC-1049-AA05-06

47. D.M. March, *Proc. Phys. Soc. A*, **279**: 420 (1964).
https://doi.org/10.1098/rspa.1964.0210

48. J. Strenberg, *J. Appl. Phys.*, **65**, No. 9: 3417 (1989).
https://doi.org/10.1063/1.342659

49. K.J. Johnson, *Contact Mechanics* (Cambridge: University Press: 1985).

50. K. Tanaka, *J. Mater. Sci.*, **22**: 1501 (1987).
https://doi.org/10.1007/BF01233154

51. D.A. Lesyk, S. Martinez, B.N. Mordyuk, V.V. Dzhemelinskyi, A. Lamikiz, and G.I. Prokopenko, *Optics and Laser Technol.*, **111**: 424 (2019).
https://doi.org/10.1016/j.optlastec.2018.09.030

52. D. Lesyk, S. Martinez, B. Mordyuk, V. Dzhemelinskyi, and O. Danyleiko, *Advances in Design, Simulation and Manufacturing II−DSMIE 2019. Lecture Notes in Mechanical Engineering* (Eds. V. Ivanov et al.) (Cham: Springer: 2020), p. 188.
https://doi.org/10.1007/978-3-030-22365-6_19

53. K.E. Grinkevich, *Trenie i Iznos*, **24**, No. 3: 100 (2003).

54. Yu.V. Mil'man, H.M. Nykyforchyn, K.E. Hrinkevych, O.T. Tsyrul'nyk, I.V. Tkachenko, V.A. Voloshyn, and L.V. Mordel, *Mater. Sci.*, **47**: 583 (2012).
https://doi.org/10.1007/s11003-012-9431-z

55. 55. K. Kato and K. Adachi, *Modern Tribology Handbook* (Ed. B. Bhushan) (Boca Raton: Taylor & Francis Group, CRC Press: 2000).

56. P.S. Bate and D.V. Wilson, *Acta Metall.*, **34**, No. 6: 1097 (1986).
https://doi.org/10.1016/0001-6160(86)90220-8

57. A.V. Byakova, Yu.V. Milman, and A.A. Vlasov, *Science of Sintering*, **36**, No. 2: 93 (2004).
https://doi.org/10.2298/SOS0402093B

58. Y. Estrin, N.V. Isaev, S.V. Lubenets, S.V. Malykhin, A.T. Pugachov, E.N. Reshetnyak, V.S. Fomenko, L.S. Fomenko, M. Janecek, and R.J. Hellmig, *Acta Mater.*, **54**, No. 20: 5581 (2006).
https://doi.org/10.1016/j.actamat.2006.07.036

59. Z. Huang, L.Y. Gu, and J.R. Weertman, *Scr. Mater.*, **37**, No. 7: 1071 (1997).
https://doi.org/10.1016/S1359-6462(97)00209-1

60. V. Popov, *Facta Universitatis. Series: Mech. Eng.*, **17**, No. 1: 39 (2019).
https://doi.org/10.22190/FUME190112007P

Ю.В. Мільман[1], *Б.М. Мордюк*[2], *К.Е. Грінкевич*[1],
С.І. Чугунова[1], *І.В. Гончарова*[1], *А.І. Лукьянов*[1], *Д.А. Лесик*[3]

[1] Інститут проблем матеріалознавства ім. І.М. Францевича НАН
  України, вул. Академіка Кржижановського, 3, 03142 Київ, Україна
[2] Інститут металофізики ім. Г.В. Курдюмова НАН України,
  бульв. Академіка Вернадського, 36, 03142 Київ, Україна
[3] Національний технічний університет України
  «Київський політехнічний інститут імені Ігоря Сікорського»,
  просп. Перемоги, 37, 03056 Київ, Україна

НОВІ МОЖЛИВОСТІ ВИЗНАЧЕННЯ ІНТЕНСИВНОСТИ ЗНОШУВАННЯ МАТЕРІАЛІВ ПРИ ТЕРТІ ЗА ДАНИМИ ІНДЕНТУВАННЯ

Статтю присвячено визначенню фізичної пластичности δ_H (відношення пластичної деформації до загальної деформації) та напруження плинности σ_S методом індентування та застосуванню цих характеристик задля аналізу інтенсивности зношування W під час тертя. Експериментальну частину роботи було виконано на крицях 9Г2Ф (AISI O2) і Х12МФ (AISI D2), поверхневі шари яких було зміцнено комбінованим термомеханічним обробленням, яке складалося з послідовного використання лазерного термічного оброблення та ультразвукового ударного оброблення. Для металів показано, що інтенсивність зношування W пропорційна фізичній пластичності δ_H й обернено пропорційна межі плинности σ_S. Запропоновано загальну схему залежности W від δ_H на основі експериментальних результатів для інструментальних криць та твердих стопів. Для криць, зношування яких спричинено пластичною деформацією, W збільшується зі збільшенням δ_H і, навпаки, зменшується для твердих стопів, які зношуються переважно механізмом руйнування. Використання фізичної пластичности δ_H і межі плинности σ_S, що обчислюються з використанням твердости та модуля Юнга, характеризує і ступінь зміцнення, й інтенсивність зношування поверхневих шарів більш повно та точніше, аніж величина твердости.

Ключові слова: зношування, фізична пластичність, межа плинности, зміцнений поверхневий шар, твердість, індентування